Cell Reports

Article

Modulation of circRNA Metabolism by m^{6}A Modification

Graphical Abstract

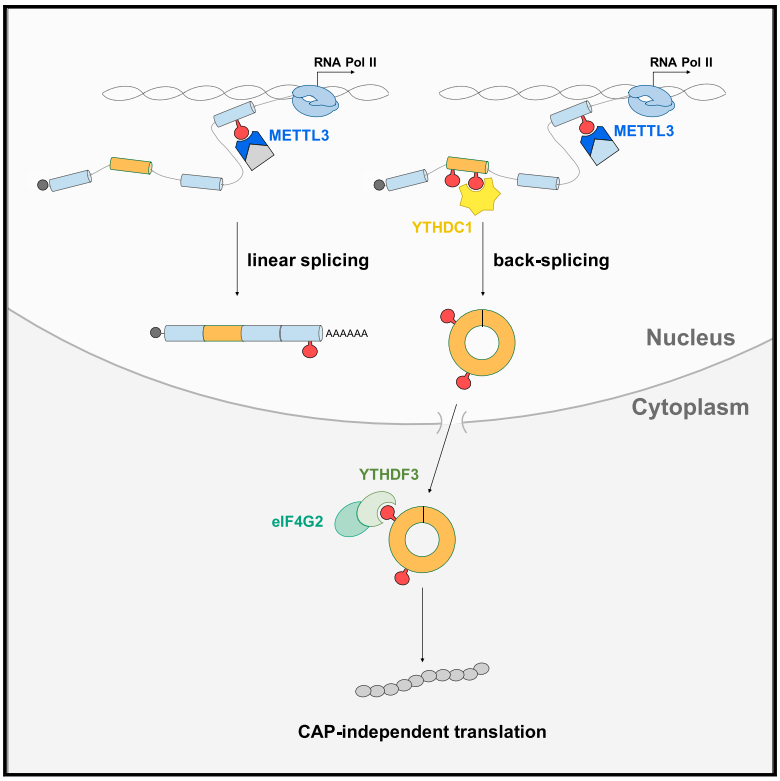

Highlights

- Specific m^{6}As control accumulation of a subset of circRNAs
- METTL3 and YTHDC1 are required to direct the biogenesis of a subset of circRNAs
- circRNAs affected by METTL3 YTHDC1 display specific m^{6}A signatures
- circ-ZNF609 translation is modulated through recognition by YTHDF3 and eIF4G2

Authors

Gaia Di Timoteo, Dario Dattilo, Alvaro Centrón-Broco, ..., Alessandro Fatica, Mariangela Morlando, Irene Bozzoni

Correspondence

irene.bozzoni@uniroma1.it

In Brief

The role of m^{6}A in the biogenesis and function of circRNAs has yet to be addressed. We discovered that METTL3 and YTHDC1 modulate the biogenesis of a subset of circRNAs, including circ-ZNF609. We show that m^{6}A regulates circZNF609 translation via YTHDF3 and eIF4G2.

Di Timoteo et al., 2020, Cell Reports *31*, 107641
May 12, 2020
https://doi.org/10.1016/j.celrep.2020.107641

CellPress

Cell Reports

CellPress
OPEN ACCESS

Article

Modulation of circRNA Metabolism by m^{6}A Modification

Gaia Di Timoteo,[1,6] Dario Dattilo,[1,6] Alvaro Centrón-Broco,[1] Alessio Colantoni,[1] Marco Guarnacci,[1] Francesca Rossi,[1] Danny Incarnato,[3] Salvatore Oliviero,[4] Alessandro Fatica,[1] Mariangela Morlando,[5] and Irene Bozzoni[1,2,7,*]

[1]Department of Biology and Biotechnology Charles Darwin, Sapienza University of Rome, Rome, Italy
[2]Center for Life Nano Science@Sapienza, Istituto Italiano di Tecnologia, Rome, Italy
[3]Groningen Biomolecular Sciences and Biotechnology Institute, Groningen, the Netherlands
[4]Department of Life Sciences and Systems Biology, University of Turin, Turin, Italy
[5]Department of Pharmaceutical Sciences, University of Perugia, Perugia, Italy
[6]These authors contributed equally
[7]Lead Contact
*Correspondence: irene.bozzoni@uniroma1.it
https://doi.org/10.1016/j.celrep.2020.107641

SUMMARY

N^6-methyladenosine (m^{6}A) is an RNA modification well-known for its contribution to different processes controlling RNA metabolism, including splicing, stability, and translation of mRNA. Conversely, the role of m^{6}A on the biogenesis and function of circular RNAs (circRNAs) has yet to be addressed. circRNAs belong to a class of covalently closed transcripts produced via a back-splicing reaction whereby a downstream 5′ splice donor site fuses to an upstream 3′ splice acceptor site. Starting from circ-ZNF609 as a study case, we discover that specific m^{6}As control its accumulation and that METTL3 and YTHDC1 are required to direct the back-splicing reaction. This feature is shared with other circRNAs because we find a significant direct correlation among METTL3 requirement, YTHDC1 binding, and the ability of m^{6}A exons to undergo back-splicing. Finally, because circ-ZNF609 displays the ability to be translated, we show that m^{6}A modifications, through recognition by YTHDF3 and eIF4G2, modulate its translation.

INTRODUCTION

N^6-methyladenosine (m^{6}A) is the most abundant internal modification of coding and non-coding RNA polymerase II transcripts, and the one with the greatest impact on their dynamic regulation. m^{6}A modification is deposited by the core heterodimeric complex composed by methyltransferase-like-3 (METTL3) and -14 (METTL14), with METTL3 being the sole catalytic subunit, and it can be reversed by the m^{6}A demethylases FTO and ALKBH5 (Zaccara et al., 2019).

m^{6}A can control any aspect of mRNA post-transcriptional regulation, including splicing, export, stability, and translation (Zaccara et al., 2019). This is achieved either by producing conformational changes within local RNA structures or by recruiting specific m^{6}A-reader proteins (Patil et al, 2018; Zaccara et al., 2019). In particular, YTH domain-containing proteins were the first readers to be identified. In human there are four YTH proteins in the cytoplasm (YTHDF1–3 and YTHDC2) and one in the nucleus (YTHDC1). Whereas YTHDFs and YTHDC2 were shown to control mRNA stability and translation, YTHDC1 was demonstrated to regulate pre-mRNA splicing and export (Zaccara et al., 2019). More recently, cytoplasmic YTH readers were also shown to favor the phase separation of m^{6}A-modified RNAs in membraneless compartments, such as stress granules and P-bodies (Ries et al., 2019).

During the splicing reaction, many pre-mRNAs can produce covalently closed circular RNAs (circRNAs), whereby a downstream 5′ splice donor site is fused to an upstream 3′ splice acceptor site in a so-called back-splicing reaction (Ashwal-Fluss et al., 2014), which is alternative to linear splicing. An open question is how the choice between the back-splicing and the linear splicing is controlled. Using circ-ZNF609 as a study case, we discovered that m^{6}A modification at specific sites can be a key element for the modulation of the two alternative pathways. Furthermore, we show that the biogenesis of a subset of circRNAs specifically requires METTL3 and YTHDC1 proteins. circ-ZNF609 is an interesting example to study because high expression levels correlate with proliferative conditions in human myoblasts and in rhabdomyosarcoma tumors, whereas its depletion decreases proliferation in both systems (Legnini et al., 2017; Rossi et al., 2019). circ-ZNF609 contains an open reading frame (ORF) and can be translated into two proteins using two alternative START codons, in a splicing-dependent and cap-independent manner by a still unidentified mechanism. Here we show that, in addition to their role in circRNA biogenesis, m^{6}A modifications on circ-ZNF609 play a relevant role in its cap-independent translation. In particular, we identified YTHDF3 and eIF4G2 proteins as important factors for mediating such a process. Altogether, these data reveal the important contribution of m^{6}A modifications to circRNA biogenesis and function.

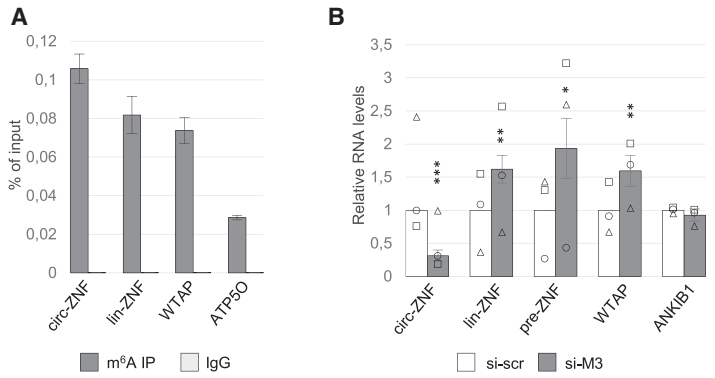

C

METTL3 KNOCK-DOWN	up-regulated circRNAs	down-regulated circRNAs
Up-regulated linear	34	50
Down-regulated linear	24	90
Not significantly altered linear	168	302
Total	226	442
Concordant (18.6%)	27.4%	72.6%
Discordant (81.4%)	35.3%	64.7%

Figure 1. METTL3 Knockdown Affects circRNA Levels

(A) Levels of circular (circ-ZNF) and linear messenger (lin-ZNF) ZNF609 RNAs recovered from immunoprecipitation with anti-m^{6}A antibody in HeLa cells expressed as percentage of input with standard deviation. WTAP and ATP5O mRNAs were used as positive and negative controls, respectively; immunoprecipitation with IgG was used as control. n = 3.

(B) Relative RNA levels of circ-ZNF, lin-ZNF, and precursor (pre-ZNF) ZNF609 RNAs upon METTL3 knockdown (si-M3) in HeLa cells. Values were normalized against ACTN1 and expressed as relative quantity with respect to scramble siRNA (si-scr) treatment set to a value of 1. WTAP and ANKIB1 RNAs were used as positive and negative controls, respectively. n = 3. The relative RNA quantity in the bars is represented as mean of the fold change with standard deviation. Dots represent the quantity relative to the endogenous control for each biological replicate. The ratio of each sample versus its experimental control was tested by two-tailed Student's t test. Student's t test-derived p values: *p < 0.05; **p < 0.01; ***p < 0.001.

(C) A table with the number of circRNAs and linear RNAs deregulated upon METTL3 knockdown is reported (p < 0.1). For each circRNA identified in the RNA-seq experiment, the $\log_2$ fold change in METTL3 knockdown along with that of its cognate linear RNA is shown in the scatterplot in Figure S1F.

RESULTS

METTL3 Knockdown Affects circRNA Levels

Similar to mRNAs, circRNAs were shown to be decorated with m^{6}A modifications and often to derive from exons that have a different methylation pattern in mRNAs (Zhou et al., 2017). By performing m^{6}A CLIP (crosslinking immunoprecipitation; Figure 1A), we found that circ-ZNF609 and its linear cognate, lin-ZNF609, were enriched in the m^{6}A-modified fraction, as observed for WTAP, used as the positive control (Sorci et al., 2018). Thereupon, we analyzed the effects of the downregulation of the main m^{6}A writer, METTL3 (Zhao et al., 2017), on the accumulation of the linear and circular transcripts originating from the *ZNF609* locus. Three different small interfering RNAs (siRNAs) against METTL3 were tested separately or in combination in HeLa cells, and all proved to be effective (Figure S1A); moreover, dot blot analysis showed that, upon METTL3 depletion with the mix of the three siRNAs (si-M3), a decrease of the overall m^{6}A levels in total RNA was obtained (Figure S1B). Upon METTL3 depletion with si-M3 (Figure S1C), we observed a strong and specific decrease of circ-ZNF609 accumulation (Figure 1B). The same results were obtained by using the three different siRNAs excluding possible off-targeting effects (Figure S1D). Unlike the circRNA, the amount of the linear ZNF609 and WTAP transcripts increased (Figure 1B), as already described for many m^{6}A-modified mRNAs whose stability is known to be negatively regulated by m^{6}A modification (Roignant and Soller, 2017; Zhao et al., 2017). Interestingly, the downregulation of circ-ZNF609 was accompanied by an increase in the levels of its unspliced precursor RNA, suggesting that the decrease in methylation could somehow affect the conversion of the pre-mRNA into the circRNA (Figure 1B).

Actinomycin D pulse chase experiments demonstrated that METTL3 depletion did not have any effect at the level of the circRNA half-life (Figure S1E); moreover, it confirmed that the circRNA has a higher stability than its linear counterpart.

Altogether, these data suggest a role of METTL3 and m^{6}A in the regulation of the back-splicing reaction, which leads to circ-ZNF609 biogenesis.

In order to understand whether this feature could be extended to other circRNAs, we performed RNA sequencing (RNA-seq) on HeLa cells depleted for METTL3. A total of 3,919 circRNAs were identified (Table S1), and among them 668 were deregulated (17%): 442 (66%) were downregulated, whereas 226 (34%) were upregulated (Figure 1C; Figure S1F; Table S1). Coherently, circ-ZNF609 was found in the downregulated group (Table S1). Differential expression analysis revealed that upon METTL3 knockdown, only 18.6% of the deregulated circRNAs had their linear counterparts significantly varying in the same direction (concordant; Figure 1C), suggesting that for the majority of circRNAs, the change in expression levels might not be associated to transcriptional regulation of their host gene. Furthermore, in most cases where the circRNA and its linear cognate displayed discordant variations, the linear isoform showed no significant changes, suggesting a specific effect on circRNA production.

In order to investigate the involvement of m^{6}A in circRNA biogenesis, we focused only on discordant circRNAs downregulated upon METTL3 depletion.

YTHDC1 Affects Back-Splicing

Because YTHDC1 was shown to be a m^{6}A reader regulating pre-mRNA splicing (Hartmann et al., 1999; Xiao et al., 2016), we tested its involvement in the back-splicing of circ-ZNF609. YTHDC1 knockdown in HeLa cells with two different siRNAs (Figure S2A) resulted in a consistent decrease of circ-ZNF609, paralleled by the increase of its precursor transcript, whereas the level of the corresponding linear mRNA remained unaltered

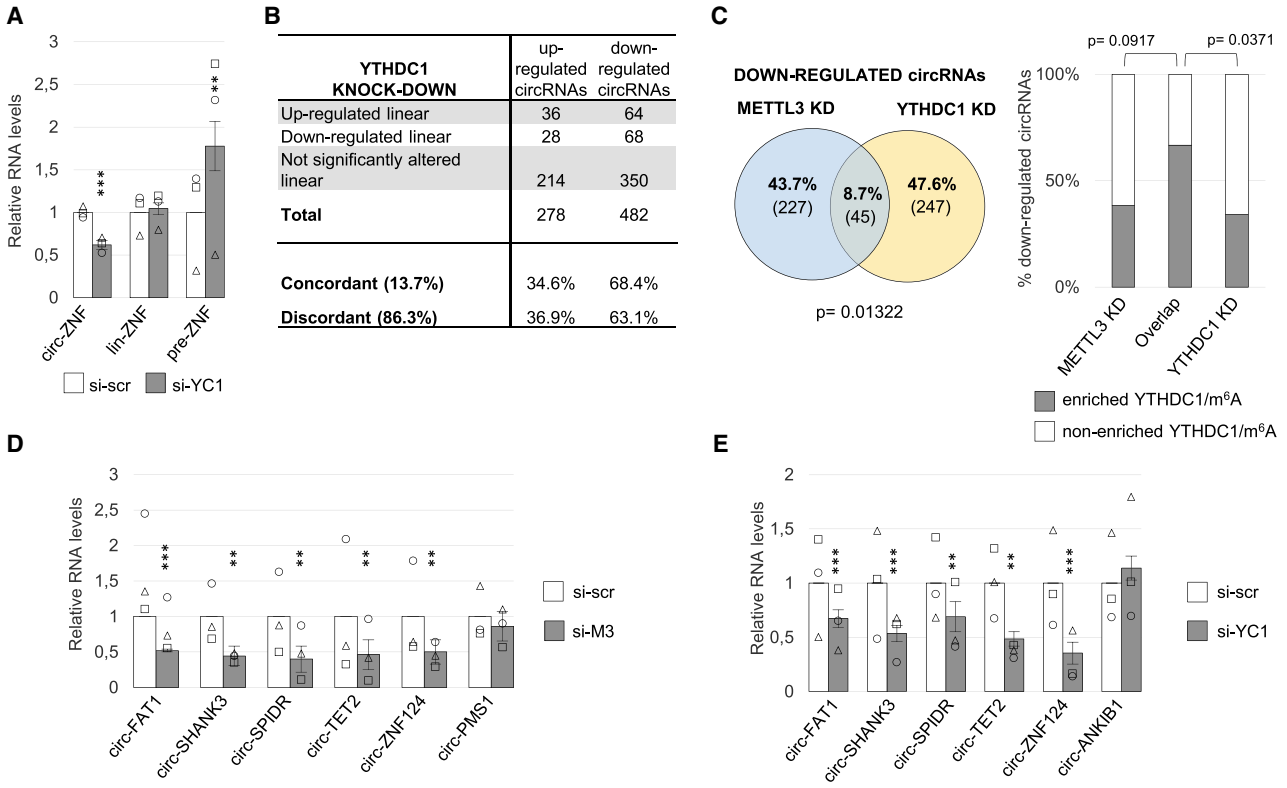

YTHDC1 KNOCK-DOWN	up-regulated circRNAs	down-regulated circRNAs
Up-regulated linear	36	64
Down-regulated linear	28	68
Not significantly altered linear	214	350
Total	278	482
Concordant (13.7%)	34.6%	68.4%
Discordant (86.3%)	36.9%	63.1%

Figure 2. YTHDC1 Affects Back-Splicing

(A) Relative RNA levels of circ-ZNF, lin-ZNF, and pre-ZNF ZNF609 RNAs upon YTHDC1 knockdown (si-YC1) in HeLa cells; values were normalized against β-Actin (ACTB) and expressed as relative quantity with respect to si-scr treatment set to a value of 1. n = 3.

(B) A table with the number of deregulated circRNAs and linear RNAs upon YTDC1 knockdown is reported ($p < 0.1$). For each circRNA identified in the RNA-seq experiment, the $\log_2$ fold change in YTHDC1 knockdown along with that of its cognate linear RNA is shown in the scatterplot in Figure S3C.

(C) Venn diagram showing the overlap between circRNAs downregulated upon METTL3 knockdown and those downregulated upon YTHDC1 knockdown. Only downregulated circRNAs identified with at least two counts in both METTL3/YTHDC1 knockdown or control samples and whose linear counterpart was not downregulated were used for this analysis. Significance was calculated via Fisher's exact test (left panel). Bar plot depicting the percentage of circRNAs downregulated upon METTL3 and/or YTHDC1 knockdown, which are also precipitated by YTHDC1 and m6A RIP (enriched YTHDC1/m^{6}A). The three bars represent the circRNAs exclusively downregulated upon METTL3 or YTHDC1 knockdown (METTL3 KD and YTHDC1 KD), as well as those that are affected by both knockdowns (overlap). p values for the differences between proportions were calculated using Pearson chi-square test with Yates continuity correction (right panel).

(D and E) Relative RNA levels of selected circRNAs showing decrease either upon METTL3 (D, si-M3) or YTHDC1 (E, si-YC1) knockdown. circ-PMS1 and circ-ANKIB1 were used as negative controls in METTL3 or YTHDC1 knockdown, respectively. Values were normalized against ACTN1 or ACTB and expressed as relative quantity with respect to si-scr treatment set to a value of 1. n = 3.

(A–E) The relative RNA quantity in the bars is represented as mean of the fold change with standard deviation. Dots represent the quantity relative to the endogenous control for each biological replicate. The ratio of each sample versus its experimental control was tested by two-tailed Student's t test. Student's t test-derived p values: *$p < 0.05$; **$p < 0.01$; ***$p < 0.001$.

(Figure 2A; Figure S2B). The same effect was also obtained in different cell lines (RD, RH4, and HEK293T), indicating that YTHDC1 regulation of circ-ZNF609 accumulation is cell type independent (Figures S2C and S2D).

Because YTHDC1 is known to have a role in the export of circRNAs (Chen et al., 2019), we tested whether the observed decrease of circ-ZNF609 could be due to a nuclear retention. As indicated in Figure S2E, the subcellular localization of circ-ZNF609 was not altered upon YTHDC1 depletion. Moreover, actinomycin D pulse chase experiments demonstrated that YTHDC1 depletion did not have any effect at the level of circRNA stability (Figure S2F). These results showed the relevance of YTHDC1 on circ-ZNF609 biogenesis and indicated that its levels are limiting for the back-splicing reaction, while not affecting either the export or the stability of the circRNA. Notably, because circ-ZNF609 levels are increased in pathological conditions where proliferation predominates above differentiation such as rhabdomyosarcoma (Rossi et al., 2019), we tested the levels of YTHDC1 in these different rhabdomyosarcoma cellular systems and found a direct correlation between circ-ZNF609 and YTHDC1 levels (Figure S2G).

Analysis of YTHDC1 RIP-seq (RNA immunoprecipitation and sequencing) data performed in HeLa cells (Roundtree et al., 2017) indicated that 78% of circRNAs, including circ-ZNF609, were enriched more than 2-fold in the immunoprecipitated fraction over the input, whereas such enrichment was not mirrored

by their linear counterparts (Figure S2H). Alongside, we found that a significant fraction of circRNAs bound by YTHDC1 (40.5%) was also present in the m^{6}A-modified RNA pool in HeLa cells (Zhou et al., 2017) (Figure S3A), whereas the overlap with circRNAs devoid of m^{6}A residues was lower than expected by chance (Figure S3B). Altogether, these data indicated a significant correlation between m^{6}A deposition and YTHDC1 binding to exons that undergo circularization.

We then performed RNA-seq in HeLa cells interfered for YTHDC1 (Figure S2A). A total of 4,809 circRNAs were identified, and among them 760 were deregulated (Table S1). Similar to what was observed in METTL3 depletion, the number of downregulated circRNAs (482) was greater than that of the upregulated ones (278; Table S1; Figure 2B; Figure S3C).

circRNAs downregulated upon YTHDC1 knockdown significantly overlapped with those precipitated both in YTHDC1 (Roundtree et al., 2017) and in m^{6}A RIP (Zhou et al., 2017, Figure S3D), reinforcing the idea of a positive effect of YTHDC1 on m^{6}A-circRNA biogenesis. Instead, no significant overlap was observed between the upregulated and the YTHDC1/m^{6}A-enriched circRNAs (Figure S3E). A small yet significant fraction of the downregulated circRNA species in YTHDC1 knockdown were in common with those decreasing upon METTL3 depletion (Figure 2C, left panel), suggesting that METTL3 and YTHDC1 could act on the same pathway to favor circRNA biogenesis. Moreover, circRNAs downregulated upon METTL3 and YTHDC1 knockdown were also enriched in YTHDC1 and m^{6}A RIP (Roundtree et al., 2017; Zhou et al., 2017) if compared with those affected independently by METTL3 or YTHDC1 (Figure 2C, right panel). On the other hand, the overlap between the circRNAs upregulated upon METTL3 and YTHDC1 depletion was not significant (Figure S3F).

We randomly selected a few circRNAs downregulated according to RNA-seq data performed upon METTL3 and YTHDC1 knockdown for quantitative RT-PCR validation. Figures 2D and 2E demonstrate that all of these circRNAs are downregulated upon the depletion of METTL3 and YTHDC1, respectively, similar to circ-ZNF609. According to RNA-seq data, circ-PMS1 and circ-ANKIB1, unaffected by METTL3 or YTHDC1 depletion, respectively, were used as negative controls. Interestingly, also in these cases, with the exception of circ-TET2, the decrease of the mature circRNA was paralleled by the increase of the precursor species in both METTL3 and YTHDC1 knockdown (Figures S3G and S3H). The analysis of the linear counterparts showed some variability upon depletion of METTL3 (Figure S3I), whereas a more homogeneous behavior was observed upon YTHDC1 depletion (Figure S3J). Finally, similar to what was observed for circ-ZNF609, YTHDC1 knockdown did not cause any circRNA mislocalization (Figure S2E), excluding possible circRNA degradation due to nuclear retention. Altogether, these data indicate that YTHDC1 acts in promoting circularization of a specific class of circRNAs.

METTL3/YTHDC1-Affected circRNAs Display Specific m^{6}A Signatures

In order to test whether the exons whose circularization is controlled by METTL3 and YTHDC1 could possess a distinctive signature of m^{6}A, we analyzed m^{6}A CLIP data obtained in HeLa cells by comparing nucleoplasmic and cytoplasmic total RNA with cytoplasmic poly(A$^+$) RNA (Ke et al., 2017). Because circRNAs should be depleted in the poly(A$^+$) fraction, the m^{6}As present only in total RNA preparations (defined as "total-only m^{6}As") can represent a bona fide circRNA signature.

Interestingly, circRNAs containing total-only m^{6}As were more represented among those decreasing upon depletion of both YTHDC1 and METTL3 compared with those affected by either METTL3 or YTHDC1 knockdown alone; moreover, this was found in both cytoplasmic and nucleoplasmic total RNA fractions (Figure 3A). This correlation suggests the hypothesis that the total-only m^{6}A signature is established in the nucleus and could act as a hallmark for METTL3/YTHDC1-dependent circRNA biogenesis.

In the same dataset, with regard to the exon from which circ-ZNF609 derives, we observed several m^{6}A modifications. Among them, the m^{6}As referred to as α, β, and γ were exclusively found in the nucleoplasmic and cytoplasmic total RNA fractions (Figure 3B), thus belonging to total-only m^{6}As.

Specific m^{6}As Control circ-ZNF609 Biogenesis

To gain further insights into the role of the m^{6}As decorating circ-ZNF609, we took advantage of an artificial construct, p-circ, which allows the overexpression of circ-ZNF609 RNA in the absence of its natural flanking introns (Legnini et al., 2017) (Figure 4A). Similar to the endogenous molecule, circ-ZNF609 derived from p-circ carried m^{6}A modifications (Figure 4B), and its accumulation decreased both upon METTL3 (Figure 4C) and YTHDC1 (Figure 4D) downregulation (Figures S4A and S4B). Notably, as for the endogenous species, YTHDC1 depletion also produced a significant increase of the unspliced precursor (Figure 4D), indicating that YTHDC1 levels were limiting also for the transcript deriving from p-circ.

Point mutations were then introduced at "As" corresponding to m^{6}A CLIP peaks, displaying either optimal m^{6}A consensus motifs or conservation in murine and human *ZNF609* exon 2 sequence (Figure 4A). As control, we raised a mutant at position 1 (c-Δ1), a canonical m^{6}A site that was not conserved and methylated in the m^{6}A CLIP dataset (Ke et al., 2017). All of the different constructs, when transfected in HeLa cells, produced unspliced poly(A$^+$) precursor transcripts, as well as the monomeric circ-ZNF609; importantly, we never observed the production of linear concatemers (Figure S4C). Single mutations at the control site 1 (c-Δ1), as well as at m^{6}A sites 2 and 3, present also in the poly(A$^+$) fraction (c-Δ2 and c-Δ3), did not show any relevant effect on circRNA accumulation, whereas double mutation at the α and β sites (c-Δα.β) had a slight effect (15%–20%; Figure 4E). Interestingly, when mutating the α and β m^{6}A sites in combination with the site at position 2 (c-Δα.β.2), we observed a dramatic drop of circRNA level (>80%) that was paralleled by a strong increase in the precursor RNA (Figure 4E), features that mirrored the endogenous situation observed upon YTHDC1 knockdown. These data showed the relevance of α and β sites for circ-ZNF609 biogenesis and indicated that, in combination with the methylation at position 2, they strongly promote the back-splicing reaction.

As a control, we analyzed the effect of the same mutations in a vector overexpressing the sequence of circ-ZNF609 in a linear

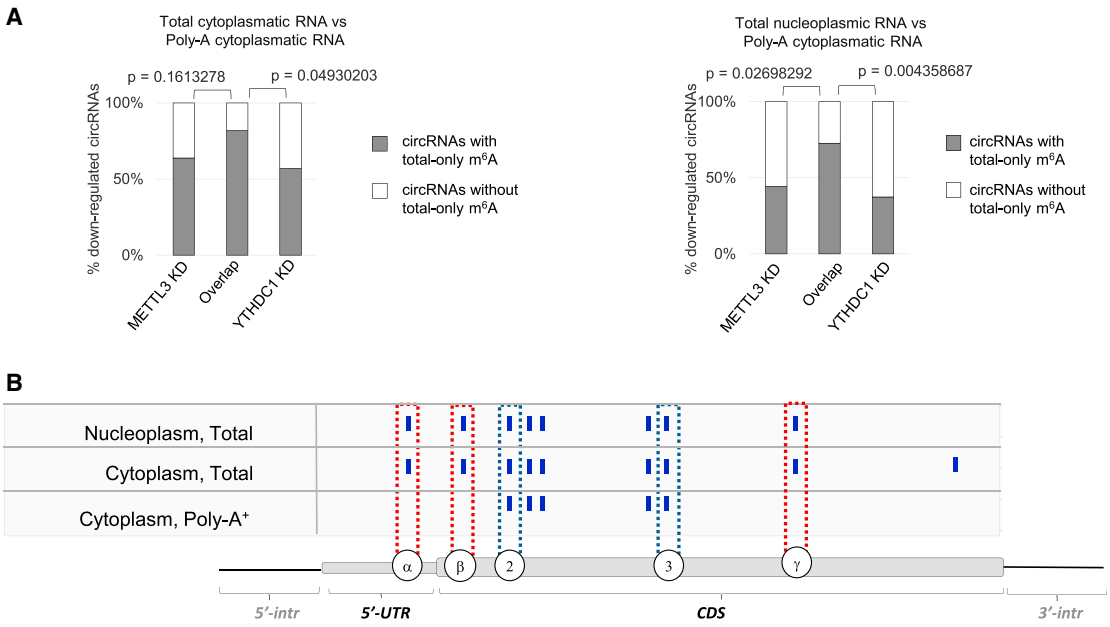

Figure 3. METTL3/YTHDC1-Affected circRNAs Contain Specific m^{6}A Signatures

(A) Bar plots depicting the fraction of downregulated circRNA exonic sequences within which m^{6}A-CLIP identified at least one m^{6}A antibody-enriched RNA region on total RNA from nucleoplasm (right) or cytoplasm (left) absent in poly(A)$^+$ RNA from cytoplasm. The three bars represent the circRNAs exclusively down-regulated upon METTL3 KD or YTHDC1 KD, as well as those that are affected by both knockdowns (overlap). p values for the differences between proportions were calculated using Pearson chi-square test with Yates continuity correction.

(B) m^{6}A sites in the exon producing circ-ZNF609 identified via m^{6}A CLIP performed on total RNA from nucleoplasm (nucleoplasm, total) and cytoplasm (cytoplasm, total) or on poly(A$^+$) RNA from cytoplasm [cytoplasm, poly(A)$^+$]. A schematic representation of the second exon of ZNF609 is shown below. 5′ UTR, coding sequence (CDS), and flanking introns (5′-intr, 3′-intr) are indicated. White circles indicate the m^{6}A sites selected for mutation; blue or red boxes highlight peaks present or not in the poly(A)$^+$ fraction, respectively.

conformation, with a cap and a poly(A) tail (p-lin, see schematic representation in Figure S4D) (Legnini et al. 2017). Notably, also the transcript originating from p-lin was enriched in the m^{6}A immunoprecipitation (Figure S4E). However, when Δ2 and Δα.β.2 mutations were introduced in p-lin, no variation was observed in the levels of the linear transcript (Figure 4F). Finally, when RNAs deriving from p-circ and c-Δα.β.2 were analyzed in cells downregulated for YTHDC1 (Figure S4B), only the wild-type transcript and not the mutant one displayed a clear responsiveness to the lack of such factor (Figure 4G), indicating that the identified m^{6}A sites are indeed sufficient for YTHDC1 activity in promoting back-splicing.

m^{6}As Control circ-ZNF609 Translation

circ-ZNF609 was previously shown to possess an ORF and to be able to undergo translation in a cap-independent manner (Legnini et al., 2017). We previously reported that an artificial *in-vitro*-synthesized circ-ZNF609, devoid of any modification, was unable to drive translation when transfected in HeLa cells (Legnini et al., 2017). Because m^{6}A modifications were shown to enable cap-independent translation (Coots et al., 2017; Meyer et al., 2015; Zhou et al., 2015), we examined their effect on circ-ZNF609. Proteins deriving from p-circ upon downregulation of METTL3 were analyzed by western blot. The evaluation of the effect of METTL3 downregulation on translation, although challenging because of the 60% decrease in circ-ZNF609 levels, appeared nevertheless higher at the protein level, reaching a further 20% decline (Figure S4A). This indicated a possible METTL3-dependent regulation of circ-ZNF609 translation.

In order to obtain data regarding the m^{6}A-dependent translational regulation of circ-ZNF609, we analyzed proteins from the same experiment shown in Figure 4E by western blot with an anti-FLAG antibody. The results showed that c-Δ2, c-Δ3, and c-Δα.β mutants displayed approximately a 50% reduction of translation when compared with p-circ or c-Δ1 (Figure 5A; Figure S5A), despite producing a comparable amount of circRNA (Figure 4E). The c-Δα.β.2 mutant displayed a strong decrease in protein production; however, due to the drastic drop in circRNA level, we could not unambiguously quantify the effect of such modifications on translation (Figure 5A; Figure S5A).

The p-lin vector expresses a transcript containing the ORF of circ-ZNF609 in a linearized conformation (Figure S4D), able to be translated in a cap-dependent manner. Notably, no translational effects were detected when selected mutations (Δ2 and Δα.β.2) were introduced in p-lin (Figure 5B; Figure S5B). These data indicate a specific function of m^{6}A in controlling translation of a circular molecule.

Due to their known role in modulating mRNA stability and translation, we tested the effects of the main YTHDF factors (1, 2, and 3) (Shi et al., 2017) on the accumulation and translation of circ-ZNF609 derived from p-circ.

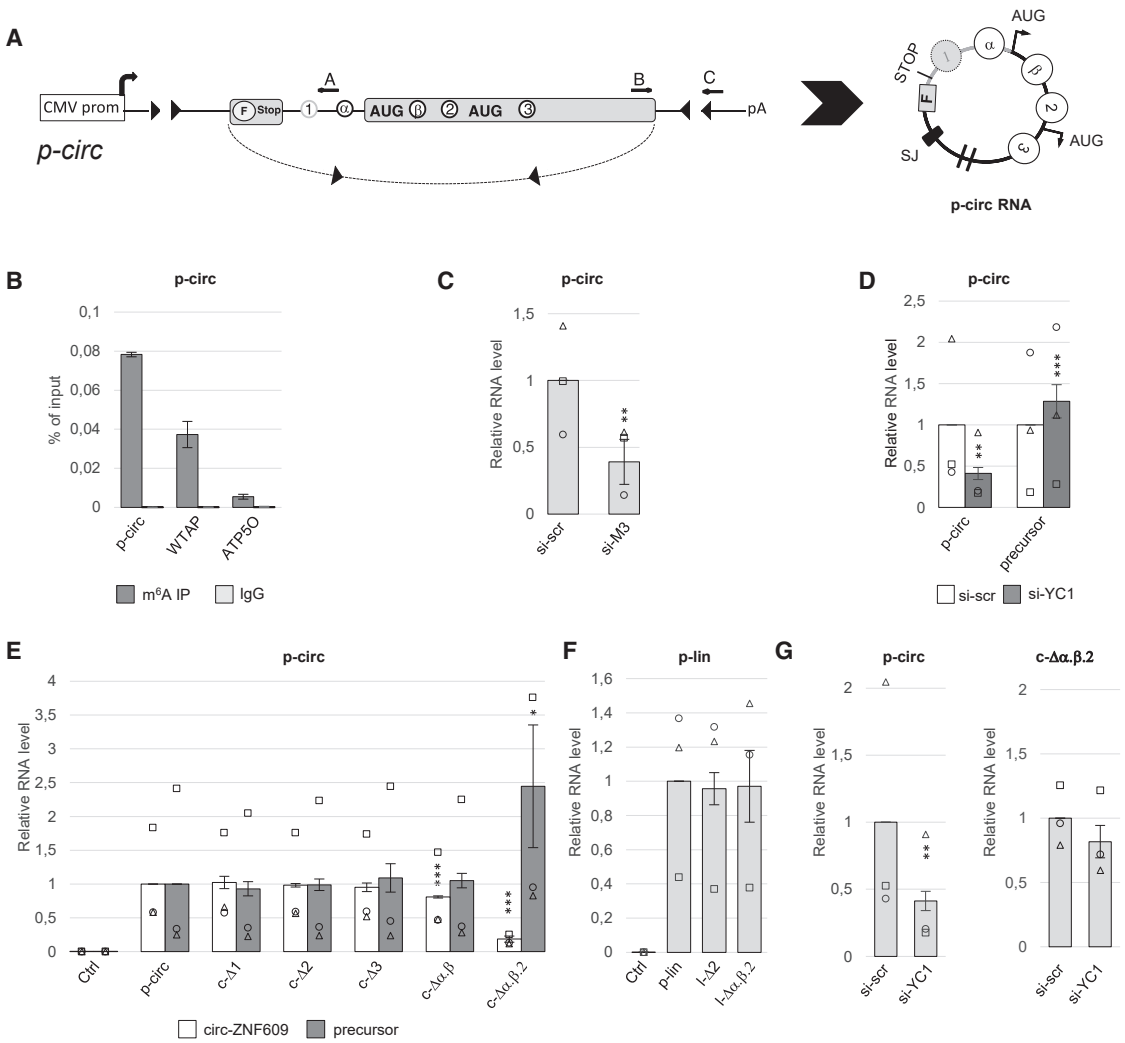

Figure 4. Specific m^{6}As Control circ-ZNF609 Biogenesis

(A) Schematic representation of the p-circ construct and the corresponding circRNA. Capital letters indicate the position of the primers used for the amplification of the mature product (*A* and *B*) or of the precursor (*B* and *C*).

(B) Levels of the transcript expressed from the p-circ construct in HeLa cells recovered from IP with anti-m^{6}A antibody, expressed as percentage of input. WTAP and ATP5O mRNAs were used as positive and negative controls, respectively; immunoprecipitation with IgG was used as control. n = 3.

(C) Relative RNA levels of the circular transcript deriving from p-circ upon METTL3 knockdown (si-M3) in HeLa cells. Values were normalized against ACTB and expressed as relative quantity with respect to si-scr treatment set to a value of 1. n = 3.

(D) Relative RNA levels of the circular transcript (p-circ) and the precursor (precursor) deriving from p-circ upon YTHDC1 knockdown (si-YC1) in HeLa cells. Values were normalized against ACTB and expressed as relative quantity with respect to si-scr treatment set to a value of 1. n = 3.

(E and F) Mutations were introduced at the m^{6}A consensus sequences in p-circ and p-lin constructs. Relative RNA levels of circular transcripts and precursor transcripts derived from p-circ (E) and the linear RNA deriving from p-lin (F), as well as from their mutant derivatives, are shown. Values were normalized against ACTB and expressed as relative quantity with respect to wild-type constructs set to a value of 1. n = 3.

(G) Relative RNA levels of the circular transcript deriving from either p-circ (already shown in Figure 4D) or c-Δα.β.2 mutant construct upon YTHDC1 knockdown (si-YC1) in HeLa cells. Values were normalized against ACTB and expressed as relative quantity with respect to si-scr treatment set to a value of 1. n = 3.

(A–G) The relative RNA quantity in the bars is represented as mean of the fold change with standard deviation. Dots represent the quantity relative to the endogenous control for each biological replicate. The ratio of each sample versus its experimental control was tested by two-tailed Student's t test. Student's t test-derived p values: *p < 0.05, **p < 0.01, ***p < 0.001.

The depletion of YTHDF1/2 had no effect on circ-ZNF609 translation (Figures 5C and 5D; Figures S5C and S5D), whereas that of YTHDF3 produced a 40% decrease (Figure 5E, panel si/p-circ; Figure S5E). Conversely, in all of the cases analyzed, no effects were seen in the accumulation level of the circRNA (Figures S5F–S5H). Notably, both protein and RNA levels derived from p-lin transcription were unaltered by YTHDF3 depletion (Figure 5E, panel si/p-lin; Figures S5I and S5J), indicating that the effect was specific for translation deriving from the circRNA. In line with these results, the overexpression of YTHDF3 resulted

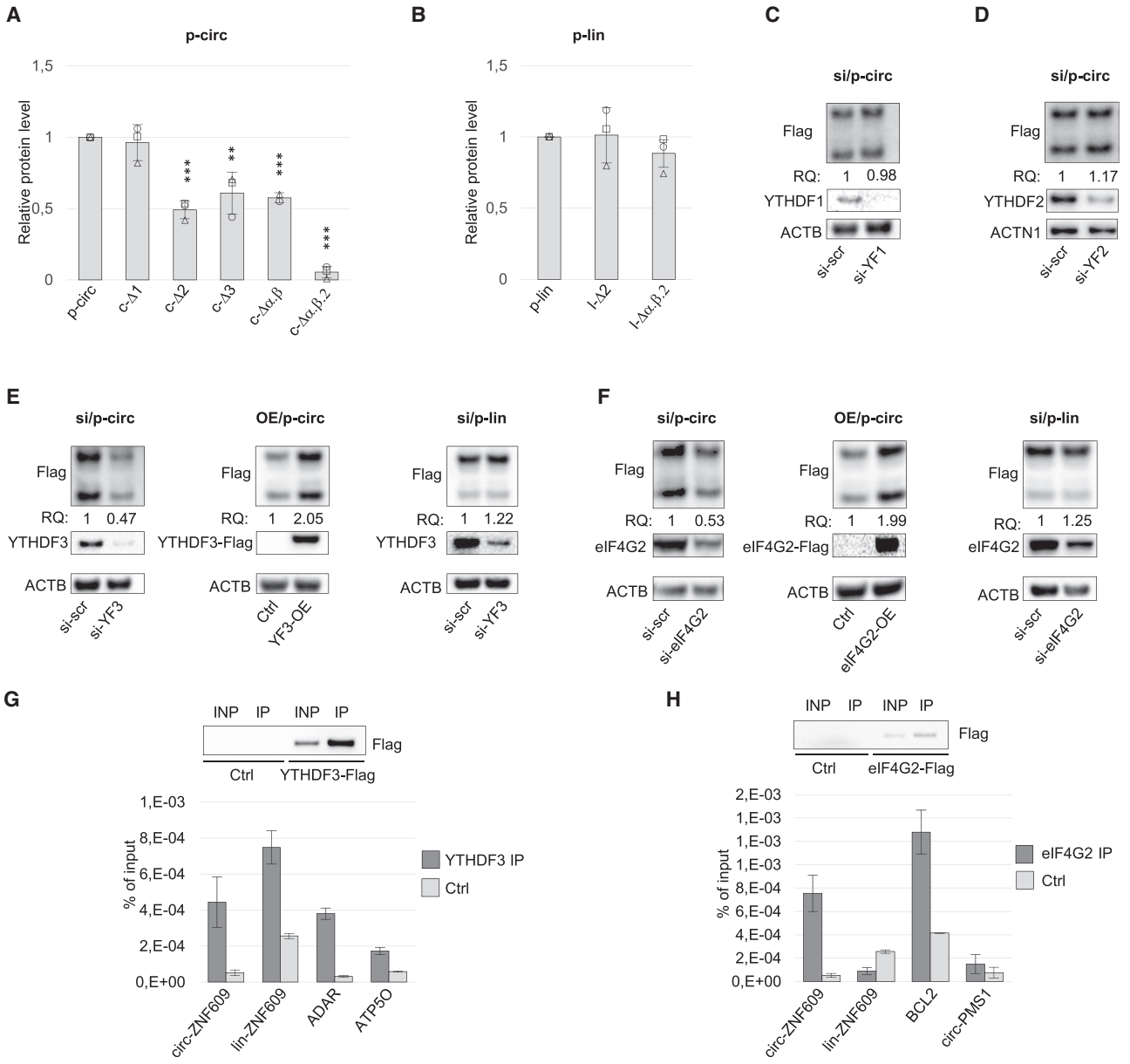

Figure 5. m^{6}As Control circ-ZNF609 Translation

(A and B) Relative protein levels deriving from circ-ZNF609 translation expressed by p-circ (A) or p-lin (B) constructs and their mutant derivatives. Levels were normalized over ACTB (p-circ) or ACTN1 (p-lin) protein level and expressed as relative quantities with respect to wild-type constructs set to 1; western blots are shown in Figures S5A and S5B. n = 3.

(C and D) Representative western blots of the proteins derived from p-circ construct upon YTHDF1 (C, si-YF1) and YTHDF2 (D, si-YF2) knockdown. The levels of YTHDF1 and YTHDF2 proteins are also shown. Relative quantities (RQs) are calculated with respect to si-scr treatment set to 1 and normalized over ACTN1 or ACTB, used as loading controls (Ctrls). n = 3.

(E and F) Representative western blots of the proteins derived from either p-circ or p-lin constructs upon YTHDF3 (E) and eIF4G2 (F) knockdown (si-YF3 and si-eIF4G2) or overexpression (YF3-OE and eIF4G2-OE); the levels of YTHDF3 and eIF4G2 proteins are also shown. RQs are calculated with respect to si-scr treatment or Ctrl set to 1 and normalized over ACTB, used as the loading Ctrl. n = 3.

(G and H) Levels of RNA recovered from IP experiments upon overexpression of FLAG-tagged YTHDF3 (G) and eIF4G2 (H). Values are expressed as percentage of input. ADAR and BCL2 mRNAs were used as positive Ctrls, whereas ATP5O and circ-PMS1 were used as negative ones in YTHDF3 and eIF4G2 IP, respectively. The IP performed in HeLa cells transfected with an empty plasmid was used as Ctrl. Representative western blots showing the IP efficiency are shown above each panel.

(A–H) The relative RNA quantity in the bars is represented as mean of the fold change with standard deviation. Dots represent the quantity relative to the endogenous Ctrl for each biological replicate. The ratio of each sample versus its experimental Ctrl was tested by two-tailed Student's t test. Student's t test-derived p values: *p < 0.05, **p < 0.01; ***p < 0.001.

in an increased translation of circ-ZNF609 (Figure 5E, panel OE/p-circ; Figure S5K), which was not justified by the increase in RNA levels (Figure S5L).

Several factors were previously shown to be associated to YTHDF3 and cap-independent translation (Zhang et al., 2019). In particular, eIF3a and eIF3b were described to bind m^{6}A residues and to initiate translation in a cap-independent manner (Meyer et al., 2015; Yang et al., 2017). However, their downregulation did not produce any observable effect on circ-ZNF609 translation (Figures S5M and S5N). Instead, eIF4G2 depletion specifically affected the translation of the circRNA derived from p-circ, but not of the linear transcript from p-lin (Figure 5F, panels si/p-circ and si/p-lin; Figures S5O and S5P). In no case was alteration of the RNA levels observed (Figures S5Q and S5R). Concordantly with YTHDF3, eIF4G2 overexpression also resulted in an increased translation of p-circ (Figure 5F, panel OE/p-circ; Figure S5S) without changes in RNA levels (Figure S5T).

In order to further support their interaction with circ-ZNF609, immunoprecipitation experiments were performed in HeLa cells, demonstrating that both YTHDF3 and eIF4G2 physically associate with the endogenous circ-ZNF609 (Figures 5G and 5H). In conclusion, these results point out the relevance of both of these factors in the translational control of circ-ZNF609.

DISCUSSION

Although the role of m^{6}A modification has been well defined in mRNA, no function for m^{6}A in circRNA biogenesis and activity has previously been shown. Here we demonstrate, using circ-ZNF609 as a study case, that m^{6}A modifications are able to control two relevant aspects of circRNA metabolism: the first correlates with the ability to regulate whether a specific exon undergoes linear or back-splicing, whereas the second correlates with that of tethering factors required for the cytoplasmic function of the circRNAs, which in our case is the cap-independent translation of circ-ZNF609.

The back-splicing reaction relies on the canonical splicing machinery in a pathway that is alternative to the production of the linear mRNA (Ashwal-Fluss et al., 2014). As in alternative splicing (AS), *cis*- and *trans*-acting factors have been shown to modulate the efficiency of back-splicing. RNA pairing between intronic sequences flanking the circularizing exon(s), such as Alu elements, favors intron looping and brings the back-splicing junctions into close proximity (Zhang et al., 2014). Specific activities have been found to control such pairing and to modulate back-splicing (Ivanov et al., 2015; Li et al., 2017). Furthermore, RNA-binding proteins can induce looping by dimerization (Conn et al., 2015) or by binding to specific motifs in the flanking introns (Errichelli et al., 2017).

In our study, we add another layer of regulation where the alternative choice between linear and circular splicing can be influenced by epitranscriptomic modifications, providing a still-missing link between m^{6}A deposition and circRNA biogenesis. Indeed, we show that for a class of circRNAs, the back-splicing reaction requires the combined action of METTL3 and YTHDC1, thus revealing an additional nuclear function for these factors. In agreement with several evidences indicating that RNA processing and m^{6}A installation are coupled, with methylation occurring co-transcriptionally (Knuckles and Bühler, 2018), we show that for a class of circRNA molecules the deposition of m^{6}A in specific exonic regions on the primary transcript correlates with their selection for the back-splicing reaction.

circ-ZNF609 was an interesting example to study because it was described to promote cell proliferation and because its levels correlate with the proliferative state of the cell. Indeed, circ-ZNF609 increases in pathological conditions such as in rhabdomyosarcoma, where proliferation predominates above differentiation (Rossi et al. 2019). Interestingly, both METTL3 and YTHDC1 paralleled the increase of circ-ZNF609 in RNA-seq data from rhabdomyosarcoma cell lines (Rossi et al. 2019), and YTHDC1 further upregulated in rhabdomyosarcoma tumors where circ-ZNF609 reaches 15-fold enrichment with respect to primary myoblasts. Altogether, these data suggest that the altered expression of METTL3 and YTHDC1 might contribute to the observed circ-ZNF609 upregulation. Although METTL3 alterations are common in tumors and in most cases a positive correlation between its expression levels and cell growth has been demonstrated (Vu et al., 2017; Ianniello et al., 2019), limited data are so far available for the m^{6}A reader YTHDC1.

To date, it is known that METTL3 can act on nascent transcripts: there is evidence that it can be recruited to the chromatin, where it can write m^{6}A on the associated precursor RNAs (Barbieri et al., 2017; Huang et al., 2019); moreover, it can interact with specific mediators or RNA binding proteins and induce m^{6}A deposition in regions close to their binding site (Patil et al., 2016; Knuckles et al., 2018). On the other hand, how specific m^{6}A consensus sites become preferentially methylated on the nascent transcript has yet to be fully ascertained.

Besides demonstrating the involvement of m^{6}A in back-splicing regulation, we also showed that m^{6}A deposition on the circularized exon is important for the cytoplasmic activity of the circRNA under study, namely, translation. In fact, circ-ZNF609 was previously shown to possess an ORF and to be translated (Legnini et al., 2017).

Several data indicate a role of m^{6}A in translation: mRNAs containing m^{6}A modification in their 5′ UTR were shown to undergo cap-independent translation upon specific cellular stress and to bypass 5′ cap-binding proteins to promote translation and to control ribosome scanning (Coots et al., 2017; Meyer et al., 2015; Zhou et al., 2018). Interestingly, eIF3 was identified as a reader of m^{6}A modifications in 5′ UTR of mRNA: consistently, genome-wide analysis showed that binding sites for this factor were shown to overlap with m^{6}A sites in 5′ UTRs (Meyer et al., 2015). However, unlike cap-independent translation of mRNA with m^{6}A-modified 5′ UTRs, we show that circ-ZNF609 translation is insensitive to eIF3 and instead relies on the YTHDF3 and eIF4G2 factors already described to drive cap-independent translation and to promote protein synthesis from artificial circRNAs (López de Quinto et al., 2001; Yang et al., 2017). Although the mechanisms of cap-independent translation initiation have been poorly understood, our results indicate that m^{6}A residues in translatable circRNAs can act as m^{6}A-induced ribosome engagement sites (MIRES), which promote cap-independent translation (Knuckles et al., 2018).

In conclusion, our data assign additional peculiar functions to m^{6}A. Because back-splicing can be considered as a form of AS, the pathways and the elements regulating such a process are expected to be similarly diverse, mirroring the complexity of factors that are involved in AS. Therefore, the finding of m^{6}A playing a crucial role in the back-splicing of a specific subset of circRNAs is in line with the heterogeneity observed for AS. Moreover, in the case of circ-ZNF609, our data also point to the existence of a specific RNA factory that controls the fate and function of the mature circRNA through modifications of the primary transcript. In addition to the above, our findings also highlight further levels of gene expression regulation controlled by m^{6}A, thus increasing the complexity and functions of transcripts deriving from a single transcriptional unit.

STAR★METHODS

Detailed methods are provided in the online version of this paper and include the following:

- KEY RESOURCES TABLE
- RESOURCE AVAILABILITY
  - Lead Contact
  - Materials Availability
  - Data and Code Availability
- EXPERIMENTAL MODEL AND SUBJECT DETAILS
  - Cell Culture
  - Patient Biopsies
- METHOD DETAILS
  - Cell Transfection
  - Protein Analyses
  - RNA Analysis
  - Plasmids Construction
  - M(6)A CLIP
  - Immunoprecipitation
  - RNA-Seq
  - Bioinformatic Analyses
- QUANTIFICATION AND STATISTICAL ANALYSIS

SUPPLEMENTAL INFORMATION

Supplemental Information can be found online at https://doi.org/10.1016/j.celrep.2020.107641.

ACKNOWLEDGMENTS

The authors acknowledge O. Sthandier and M. Marchioni for technical help; V. Silenzi for reading the manuscript; C. Dominici and F. Megiorni for biological samples; C. He, M. Sorci, Z. Ianniello, and L. Ceci Ginistrelli for providing materials; and I. Legnini for discussion. A.C.-B. is a recipient of a H2020-MSCA-ITN-2016 (GA 721890). This work was partially supported by grants from ERC-2019-SyG (855923-ASTRA to I.B.), Telethon (GGP16213 to I.B.), AIRC (IG 2019 Id. 23053 to I.B.; IG 2017 Id.20240 to S.O.), and PRIN 2017 (2017P352Z4 to I.B. and S.O.). The authors wish to dedicate this manuscript to all researchers, volunteers, and people in healthcare organizations operating around the world to fight coronavirus disease 2019 (COVID-19) infections.

AUTHOR CONTRIBUTIONS

G.D.T., D.D., M.M., and I.B. designed and conceived the study. The experiments were performed and analyzed by G.D.T., D.D., M.G., F.R., and D.I. Bioinformatics data analysis was performed by A.C., A.C.-B., and D.I. The original draft of the manuscript was written by I.B., G.D.T., and D.D., with major contributions from A.C., A.F., and M.M., and with suggestions from all of the other authors. I.B. and S.O. supervised the project.

DECLARATION OF INTERESTS

The authors declare no competing interests.

Received: November 25, 2019
Revised: February 24, 2020
Accepted: April 22, 2020
Published: May 12, 2020

REFERENCES

Ashwal-Fluss, R., Meyer, M., Pamudurti, N.R., Ivanov, A., Bartok, O., Hanan, M., Evantal, N., Memczak, S., Rajewsky, N., and Kadener, S. (2014). circRNA biogenesis competes with pre-mRNA splicing. Mol. Cell *56*, 55–66.

Barbieri, I., Tzelepis, K., Pandolfini, L., Shi, J., Millán-Zambrano, G., Robson, S.C., Aspris, D., Migliori, V., Bannister, A.J., Han, N., et al. (2017). Promoter-bound METTL3 maintains myeloid leukaemia by m^{6}A-dependent translation control. Nature *552*, 126–131.

Bolger, A.M., Lohse, M., and Usadel, B. (2014). Trimmomatic: a flexible trimmer for Illumina sequence data. Bioinformatics *30*, 2114–2120.

Chen, R.-X., Chen, X., Xia, L.-P., Zhang, J.-X., Pan, Z.-Z., Ma, X.-D., Han, K., Chen, J.-W., Judde, J.-G., Deas, O., et al. (2019). *N*^{6}-methyladenosine modification of circNSUN2 facilitates cytoplasmic export and stabilizes *HMGA2* to promote colorectal liver metastasis. Nature Communications *10*, 4695.

Conn, S.J., Pillman, K.A., Toubia, J., Conn, V.M., Salmanidis, M., Phillips, C.A., Roslan, S., Schreiber, A.W., Gregory, P.A., and Goodall, G.J. (2015). The RNA binding protein quaking regulates formation of circRNAs. Cell *160*, 1125–1134.

Coots, R.A., Liu, X.M., Mao, Y., Dong, L., Zhou, J., Wan, J., Zhang, X., and Qian, S.B. (2017). m^{6}A Facilitates eIF4F-Independent mRNA Translation. Mol. Cell *68*, 504–514.e7.

Errichelli, L., Dini Modigliani, S., Laneve, P., Colantoni, A., Legnini, I., Capauto, D., Rosa, A., De Santis, R., Scarfò, R., Peruzzi, G., et al. (2017). FUS affects circular RNA expression in murine embryonic stem cell-derived motor neurons. Nat. Commun. *8*, 14741.

Gao, Y., Zhang, J., and Zhao, F. (2018). Circular RNA identification based on multiple seed matching. Brief. Bioinform. *19*, 803–810.

Hartmann, A.M., Nayler, O., Schwaiger, F.W., Obermeier, A., and Stamm, S. (1999). The interaction and colocalization of Sam68 with the splicing-associated factor YT521-B in nuclear dots is regulated by the Src family kinase p59(fyn). Mol. Biol. Cell *10*, 3909–3926.

Huang, H., Weng, H., Zhou, K., Wu, T., Zhao, B.S., Sun, M., Chen, Z., Deng, X., Xiao, G., Auer, F., et al. (2019). Histone H3 trimethylation at lysine 36 guides m^{6}A RNA modification co-transcriptionally. Nature *567*, 414–419.

Ianniello, Z., Paiardini, A., and Fatica, A. (2019). N^6-Methyladenosine (M^{6}A): A promising new molecular target in acute myeloid leukemia. Front. Oncol. *9*, 251.

Ivanov, A., Memczak, S., Wyler, E., Torti, F., Porath, H.T., Orejuela, M.R., Piechotta, M., Levanon, E.Y., Landthaler, M., Dieterich, C., and Rajewsky, N. (2015). Analysis of intron sequences reveals hallmarks of circular RNA biogenesis in animals. Cell Rep. *10*, 170–177.

Ke, S., Pandya-Jones, A., Saito, Y., Fak, J.J., Vågbø, C.B., Geula, S., Hanna, J.H., Black, D.L., Darnell, J.E., Jr., and Darnell, R.B. (2017). m^{6}A mRNA modifications are deposited in nascent pre-mRNA and are not required for splicing but do specify cytoplasmic turnover. Genes Dev. *31*, 990–1006.

Knuckles, P., and Bühler, M. (2018). Adenosine methylation as a molecular imprint defining the fate of RNA. FEBS Lett. *592*, 2845–2859.

Knuckles, P., Lence, T., Haussmann, I.U., Jacob, D., Kreim, N., Carl, S.H., Masiello, I., Hares, T., Villaseñor, R., Hess, D., et al. (2018). Zc3h13/Flacc is required for adenosine methylation by bridging the mRNA-binding factor

Rbm15/Spenito to the m^{6}A machinery component Wtap/Fl(2)d. Genes Dev. *32*, 415–429.

Legnini, I., Di Timoteo, G., Rossi, F., Morlando, M., Briganti, F., Sthandier, O., Fatica, A., Santini, T., Andronache, A., Wade, M., et al. (2017). Circ-ZNF609 Is a Circular RNA that Can Be Translated and Functions in Myogenesis. Mol. Cell *66*, 22–37.e9.

Li, H. (2013). Aligning sequence reads, clone sequences and assembly contigs with BWA-MEM. arXiv, arXiv:1303.3997. https://arxiv.org/abs/1303.3997.

Li, X., Liu, C.X., Xue, W., Zhang, Y., Jiang, S., Yin, Q.F., Wei, J., Yao, R.W., Yang, L., and Chen, L.L. (2017). Coordinated circRNA Biogenesis and Function with NF90/NF110 in Viral Infection. Mol. Cell *67*, 214–227.e7.

Linder, B., Grozhik, A.V., Olarerin-George, A.O., Meydan, C., Mason, C.E., and Jaffrey, S.R. (2015). Single-nucleotide-resolution mapping of m6A and m6Am throughout the transcriptome. Nat. Methods *12*, 767–772.

López de Quinto, S., Lafuente, E., and Martínez-Salas, E. (2001). IRES interaction with translation initiation factors: functional characterization of novel RNA contacts with eIF3, eIF4B, and eIF4GII. RNA *7*, 1213–1226.

Martin, M. (2011). Cutadapt removes adapter sequences from high-throughput sequencing reads. EMBnet. J. *17*, 10–12.

Megiorni, F., Camero, S., Ceccarelli, S., McDowell, H.P., Mannarino, O., Marampon, F., Pizer, B., Shukla, R., Pizzuti, A., Marchese, C., et al. (2016). DNMT3B in vitro knocking-down is able to reverse embryonal rhabdomyosarcoma cell phenotype through inhibition of proliferation and induction of myogenic differentiation. Oncotarget *7*, 79342–79356.

Meyer, K.D., Patil, D.P., Zhou, J., Zinoviev, A., Skabkin, M.A., Elemento, O., Pestova, T.V., Qian, S.B., and Jaffrey, S.R. (2015). 5′ UTR m(6)A Promotes Cap-Independent Translation. Cell *163*, 999–1010.

Patil, D.P., Chen, C.K., Pickering, B.F., Chow, A., Jackson, C., Guttman, M., and Jaffrey, S.R. (2016). m(6)A RNA methylation promotes XIST-mediated transcriptional repression. Nature *537*, 369–373.

Patil, D.P., Pickering, B.F., and Jaffrey, S.R. (2018). Reading m^{6}A in the Transcriptome: m^{6}A-Binding Proteins. Trends Cell Biol. *28*, 113–127.

Quinlan, A.R., and Hall, I.M. (2010). BEDTools: A Flexible Suite of Utilities for Comparing Genomic Features. Bioinformatics *26*, 841–842.

Ries, R.J., Zaccara, S., Klein, P., Olarerin-George, A., Namkoong, S., Pickering, B.F., Patil, D.P., Kwak, H., Lee, J.H., and Jaffrey, S.R. (2019). m^{6}A enhances the phase separation potential of mRNA. Nature *571*, 424–428.

Robinson, M.D., McCarthy, D.J., and Smyth, G.K. (2010). edgeR: a Bioconductor package for differential expression analysis of digital gene expression data. Bioinformatics *26*, 139–140.

Roignant, J.Y., and Soller, M. (2017). m6A in mRNA: An Ancient Mechanism for Fine-Tuning Gene Expression. Trends Genet. *33*, 380–390.

Rossi, F., Legnini, I., Megiorni, F., Colantoni, A., Santini, T., Morlando, M., Di Timoteo, G., Dattilo, D., Dominici, C., and Bozzoni, I. (2019). Circ-ZNF609 regulates G1-S progression in rhabdomyosarcoma. Oncogene *38*, 3843–3854.

Roundtree, I.A., Luo, G.Z., Zhang, Z., Wang, X., Zhou, T., Cui, Y., Sha, J., Huang, X., Guerrero, L., Xie, P., et al. (2017). YTHDC1 mediates nuclear export of N^6-methyladenosine methylated mRNAs. eLife *6*, e31311.

Shi, H., Wang, X., Lu, Z., Zhao, B.S., Ma, H., Hsu, P.J., Liu, C., and He, C. (2017). YTHDF3 facilitates translation and decay of N^6-methyladenosine-modified RNA. Cell Res. *27*, 315–328.

Sorci, M., Ianniello, Z., Cruciani, S., Larivera, S., Ginistrelli, L.C., Capuano, E., Marchioni, M., Fazi, F., and Fatica, A. (2018). METTL3 regulates WTAP protein homeostasis. Cell Death Dis. *9*, 796.

Vu, L.P., Pickering, B.F., Cheng, Y., Zaccara, S., Nguyen, D., Minuesa, G., Chou, T., Chow, A., Saletore, Y., MacKay, M., et al. (2017). The N^6-methyladenosine (m^{6}A)-forming enzyme METTL3 controls myeloid differentiation of normal hematopoietic and leukemia cells. Nat. Med. *23*, 1369–1376.

Xiao, W., Adhikari, S., Dahal, U., Chen, Y.S., Hao, Y.J., Sun, B.F., Sun, H.Y., Li, A., Ping, X.L., Lai, W.Y., et al. (2016). Nuclear m(6)A Reader YTHDC1 Regulates mRNA Splicing. Mol. Cell *61*, 507–519.

Yang, Y., Fan, X., Mao, M., Song, X., Wu, P., Zhang, Y., Jin, Y., Yang, Y., Chen, L.L., Wang, Y., et al. (2017). Extensive translation of circular RNAs driven by N^6-methyladenosine. Cell Res. *27*, 626–641.

Zaccara, S., Ries, R.J., and Jaffrey, S.R. (2019). Reading, writing and erasing mRNA methylation. Nat. Rev. Mol. Cell Biol. *20*, 608–624.

Zerbino, D.R., Achuthan, P., Akanni, W., Amode, M.R., Barrell, D., Bhai, J., Billis, K., Cummins, C., Gall, A., and García Girón, C. (2018). Ensembl 2018. Nucleic Acids Res. *46*, D754–D761.

Zhang, X.-O., Wang, H.B., Zhang, Y., Lu, X., Chen, L.L., and Yang, L. (2014). Complementary sequence-mediated exon circularization. Cell *159*, 134–147.

Zhang, Y., Wang, X., Zhang, X., Wang, J., Ma, Y., Zhang, L., and Cao, X. (2019). RNA-binding protein YTHDF3 suppresses interferon-dependent antiviral responses by promoting FOXO3 translation. Proc. Natl Acad. Sci. USA *116*, 976–981.

Zhao, B.S., Roundtree, I.A., and He, C. (2017). Post-transcriptional gene regulation by mRNA modifications. Nat. Rev. Mol. Cell Biol. *18*, 31–42.

Zhou, J., Wan, J., Gao, X., Zhang, X., Jaffrey, S.R., and Qian, S.B. (2015). Dynamic m(6)A mRNA methylation directs translational control of heat shock response. Nature *526*, 591–594.

Zhou, C., Molinie, B., Daneshvar, K., Pondick, J.V., Wang, J., Van Wittenberghe, N., Xing, Y., Giallourakis, C.C., and Mullen, A.C. (2017). Genome-Wide Maps of m6A circRNAs Identify Widespread and Cell-Type-Specific Methylation Patterns that Are Distinct from mRNAs. Cell Rep. *20*, 2262–2276.

Zhou, J., Wan, J., Shu, X.E., Mao, Y., Liu, X.M., Yuan, X., Zhang, X., Hess, M.E., Brüning, J.C., and Qian, S.B. (2018). N^6-Methyladenosine Guides mRNA Alternative Translation during Integrated Stress Response. Mol. Cell *69*, 636–647.e7.

STAR★METHODS

KEY RESOURCES TABLE

REAGENT or RESOURCE	SOURCE	IDENTIFIER
Antibodies		
mouse monoclonal anti-Flag M2	Sigma-Aldrich	Cat#F1804-1M, RRID:AB_259529
mouse monoclonal anti-FLAG® M2-Peroxidase (HRP)	Sigma-Aldrich	Cat#A8592-2MG, RRID:AB_439702
rabbit monoclonal METTL3	Abcam	Cat# ab195352, RRID:AB_2721254
rabbit polyclonal YTHDF1	Abcam	Cat#ab99080, RRID:AB_10675362
rabbit polyclonal YTHDF2	ProteinTech	Cat#24744-1-AP, RRID:AB_2687435
rabbit polyclonal YTHDF3	ProteinTech	Cat#25537-1-AP, RRID:AB_2847817
rabbit polyclonal eIF4G2	Atlas Antibodies	Cat#HPA016965, RRID:AB_1848100
rabbit polyclonal Actinin H-300	Santa Cruz Biotechnology	Cat#sc-15335, RRID:AB_2223809
mouse monoclonal ACTB monoclonal Anti-®-Actin−Peroxidase clone AC-15	Sigma	Cat#A3854, RRID:AB_262011
rabbit polyclonal eIF3B/EIF3S9	Bethyl	Cat#A301-761A, RRID:AB_1210995
rabbit polyclonal eIF3A/eIF3S10	Bethyl	Cat#A302-002A-M, RRID:AB_2780269
rabbit polyclonal YTHDC1	Abcam	Cat#ab122340, RRID:AB_11128253
mouse monoclonal GAPDH (6C5)	Santa Cruz Biotechnology	Cat#sc-32233, RRID:AB_627679
Bacterial and Virus Strains		
Subcloning efficiency DH5α competent cells	Thermo Fisher Scientific	cat#18265017
Biological Samples		
tumor biopsy from primary ERMS	Department of Oncology at Alder Hey Children's NHS Foundation Trust, Liverpool, United Kingdom	see method details
Chemicals, Peptides, and Recombinant Proteins		
DMEM-High glucose	sigma-Aldrich	cat#D6546
FBS	sigma-Aldrich	cat#F7524
L-glutamine	sigma-Aldrich	cat#G7513
EGF	Corning	cat#354052
penicillin/strepromycin	sigma-Aldrich	cat#P0781
FGFb	Millipore-MERCK	cat#01-106
insulin	sigma-Aldrich	cat#11376497001
Opti-MEM I	Thermo Fisher Scientific	cat#31985047
Lipofectamine 2000	Thermo Fisher Scientific	cat#11668019
Lipofectamine RNAiMax	Thermo Fisher Scientific	cat#13778150
cOmplete, EDTA-free PIC	Roche	cat#11873580001
NuPage 4-12% Bis-Tris-Gel	Thermo Fisher Scientific	cat#NP0321BOX
NuPage MES SDS running buffer 20x	Thermo Fisher Scientific	cat#NP0002
NuPage Transfer buffer 20x	Thermo Fisher Scientific	cat#NP0006
4xLaemmli sample buffer	Biorad	cat#1610747
PBS	Sigma-Aldrich	N/A
RNase inhibitors	Thermo Fischer Scientific	Cat# EO0384
Dynabeads protein A/protein G	Thermo Fischer Scientific	cat#10015D
Anti-FLAG Magnetic Beads	Sigma	cat#M8823
VILO Superscript	Thermo Fisher Scientific	Cat# 11754050
Qiazol reagent	QIAGEN	Cat# 79306
PrimeScript RT Master Mix	TakaraBio	cat#RR036b
LiteAblot Extend Long Lasting Chemiluminescent Substrate	EuroClone	cat#EMP013001

(*Continued on next page*)

Continued

REAGENT or RESOURCE	SOURCE	IDENTIFIER
Clarity Max Western ECL Substrate	BioRad	cat#1705062
T4 RNA Ligase 1	BioLabs	Cat# M0204S
DNase	Thermo Fischer Scientific	Cat#EN0525
MyTaq DNA Polimerase	Bioline	cat#BIO-21105
Critical Commercial Assays		
In-Fusion HD Cloning Kit	Clontech	Cat#639649
Paris Kit	Thermo Fisher Scientific	cat#AM1921
Direct-Zol RNA MiniPrep Kit	Zymo Research	cat#R2050
Deposited Data		
YTHDC1 RIP-Seq raw data	see method details	GEO: GSE74397
m^6A RIP raw data	see method details	GEO: GSE85324
m^6a-CLIP	see method details	GEO: GSE86336
METTL3 KD RNA sequencing raw data	this paper	GEO: GSE139076
YTHDC1 KD RNA sequencing raw data	this paper	GEO: GSE139076
Experimental Models: Cell Lines		
Human male myoblasts (WT)	Telethon Biobank	N/A
RD	ATCC	CCL-136
RH4	see cell culture	N/A
HeLa	ATCC	CCL-2
HEK293T	ATCC	CRL-3216
Oligonucleotides		
DNA oligonucleotides used in this work are listed in Table S2	this paper	
siRNAs used in this work are listed in Table S2	this paper	
Recombinant DNA		
pcDNA3.1(-)	Thermo Fisher Scientific	N/A
p-circ	see plasmid construction	N/A
p-lin	see plasmid construction	N/A
c-Δ1	this paper	N/A
c-Δ2	this paper	N/A
l-Δ2	this paper	N/A
c-Δ3	this paper	N/A
c-Δα.β	this paper	N/A
c-Δα.β.2	this paper	N/A
l-Δα.β.2	this paper	N/A
Flag-tagged YTHDF3	see plasmid costruction	N/A
Flag-tagged EIF4G2	Sino Biological Inc.	HG16622-CF
Software and Algorithms		
ImageLab software	Biorad	https://www.bio-rad.com/it-it/product/image-lab-software?ID=KRE6P5E8Z
Trimmomatic version 0.322.0.6	Bolger et al., 2014	http://www.usadellab.org/cms/?page=trimmomatic
Cutadapt version 1.4.2	Martin, 2011	https://cutadapt.readthedocs.io/en/stable/
BWA version 0.7.10-r789	Li, 2013	http://bio-bwa.sourceforge.net/
CIRI version 2.0.6	Gao et al., 2018	https://sourceforge.net/projects/ciri/files/CIRI2/
R version 3.5.2	R Core Team, 2017	https://www.r-project.org/
edgeR version 3.24.3	Robinson et al., 2010	https://bioconductor.org/packages/release/bioc/html/edgeR.html
Bedtools version 2.21.0	Quinlan and Hall, 2010	https://github.com/arq5x/bedtools2

RESOURCE AVAILABILITY

Lead Contact

Further information and requests for resources and reagents should be directed to and will be fulfilled by the Lead Contact, Irene Bozzoni (irene.bozzoni@uniroma1.it)

Materials Availability

All unique/stable reagents generated in this study are available from the lead contact.

Data and Code Availability

All software used in this manuscript is listed in the Key Resources Table. Additional dedicated scripts developed for this work are available upon request. The accession number for the high-throughput sequencing data reported in this paper is GEO : GSE139076.

EXPERIMENTAL MODEL AND SUBJECT DETAILS

Cell Culture

Wild-type human primary myoblasts (Telethon Biobank) were obtained from a skeletal muscle biopsy from a 2-year-old male child. No information available about their authentication. They were cultured in growth medium (GM): DMEM high glucose (Sigma-Aldrich, Saint Louis, MO, USA), 10% FBS (Sigma-Aldrich), L-glutammine (Sigma-Aldrich) 2 mM, insulin (Sigma-Aldrich) 50 mg/ml, FGFb (Millipore-Merck) 25 ng/ml, EGF (Corning, Corning, NY, USA) 1 ng/ml, penicillin-streptomycin 1 × (Sigma-Aldrich). Human ERMS RD cell line (embryonal rhabdomyosarcoma cell line from a female patient) and ARMS RH4 cells line (alveolar rhabdomyosarcoma cell line from a female patient), HEK293T (human embryonal kidney cell line) as well as HeLa (Adenocarcinoma cell line from a female patient) cells were cultured in DMEM (Sigma-Aldrich) supplemented with 10% FBS (Sigma-Aldrich), L-glutammine (Sigma-Aldrich) 2 mM and penicillin-streptomycin (Sigma-Aldrich). RD and RH4 cell lines were the same as Megiorni et al. (2016). and Rossi et al. (2019) were previously authenticated and described in Megiorni et al. (2016). All cells were cultured at 37°C in a humidified atmosphere of 5% CO_2.

Patient Biopsies

The tumor sample from a primary ERMS was obtained at diagnosis before any treatment from children admitted to the Department of Oncology at Alder Hey Children's NHS Foundation Trust, Liverpool, United Kingdom. Institutional written informed consent was obtained from the patient's parents or legal guardians. The study underwent ethical review and approval according to the local institutional guidelines (Alder Hey Children's NHS Foundation Trust Ethics Committee, approval number 09/H1002/88).

METHOD DETAILS

Cell Transfection

Cells (150-200x10^3) were plated in 35mm plates and transfected 12hrs later with the siRNA against the target selected or the negative control (final concentration 30nM) using 5 μL of Lipofectamine RNAiMAX Reagent (Thermo Fisher Scientific) and 300 μL of Opti-MEM (Thermo Fisher Scientific). The medium was replaced 5-12hrs later. Cells were harvested 48hrs later. Exceptionally for the knockdown of METTL3 cells were instead treated with a second siRNA pulse 48hrs after the first transfection. For actinomycin treatment, cells depleted for YTHDC1 and METTL3 were split into two different plates and, after 12h, harvested or kept in their medium added with actinomycin (5mg/ml) for 6.5h. Plasmids transfections were performed on untreated cells or, when required, 12hrs after the siRNA transfections using 3 μL of Lipofectamine 2000 (Life technologies) in 300 μL of Opti-MEM (Thermo Fisher Scientific) with 100 ng-3 μg of DNA, added to a 35-mm plate with 150-200x10^3 cells in 2 mL of medium. Medium was replaced 6-12hr after the transfection and cells harvested for protein and RNA analyses 48hr later.

For the cells treated with either the siRNA against METTL3, plasmid transfection was performed 24hrs after the siRNA transfection.

Protein Analyses

Cells were harvested with 50-150 μL of Protein Extraction Buffer (100 mM Tris pH7.5, EDTA 1mM, SDS 2%, PIC1X (Complete, EDTA free, Roche) and incubated 10min on ice, then incubated on a rotator for 30min at 4°C and centrifuged at 13000xrpm for 10min at 4°C.

The supernatant was transferred to a clean tube, used or stored at −80°C. Total protein concentration was measured through the Bradford reagent (Bio-Rad Protein Assay) following manufacturer's instructions.

25-50 μg of proteins were loaded on 4%–12% bis-tris-acrylamide gel (Life technologies) and transferred to a nitrocellulose membrane. The membrane was blocked in 5% milk and then hybridized with specific antibodies for 2hrs-o.n. at room temperature. After three washes in TBST, the filter was hybridized with the corresponding secondary antibody, if required, for one hour at room temperature.

Protein detection was carried out with LiteAblot®EXTEND Long Lasting Chemiolominescent Substrate (EuroClone) or with Clarity Max Western ECL Blotting Substrate (BioRad) using ChemiDoc MP System and images were analyzed using Image Lab Software (BioRad).

RNA Analysis

Cell fractionation was carried out thanks to Ambion PARIS kit according to manufacturer's protocol.

Nuclear, cytoplasmic or total RNA in this study was extracted with Quiazol reagent and the Direct-zol RNA Miniprep (Zymo Research) kit according to the manufacturer's specifications. When needed, DNase treatment was performed (Thermo Fisher Scientific).

Reverse transcription reactions of this study were performed with PrimeScript RT Master Mix (Takara Bio) on 100-500ng of total RNA in a 10 μL reaction. QPCR analyses in this study were performed with 6-15ng equivalent of cDNA, 7.5 μL of 2X SYBR Mastermix (QIAGEN), 1.5 μL of 5 μM primers and water to a final volume of 15 μl. DNA amplification (40 cycles of 95°C for 30 s, 55°C for 30 s and 72°C for 30 s, followed by melting curve analysis) was monitored with an ABI 7500 Fast or StepOnePlus System qPCR instrument.

PCR reactions were performed with 0.3 μL of Mytaq DNA polymerase (Bioline) in 25 μL water with 5 μL of 5X reaction buffer, 6-15ng of cDNA, 2.5 μL of 5 μM primers. Reaction was carried out for 30 cycles at 95°C for 25 s, 55°C for 25 s, 72°C for 25 s. 5 μL of PCR were run on 2% agarose gel. All primers used in this study are reported below.

Relative RNA quantity was calculated as the fold change (ΔΔCt) with respect to the experimental control sample set as 1. Dots represent the quantity relative to the endogenous control (ΔCt) and normalized over ACTN1 or ACTB or GAPDH mRNA. The ratio of each sample versus its experimental control was tested by two-tailed Student's t test. One asterisk indicates a Student's t test-derived p value < 0.05, two asterisks indicate a p value < 0.01, and three asterisks a p value < 0.001. For dot-blot analysis, RNA samples were denatured at 95°C for 5 min and loaded onto nitrocellulose membrane using the Bio-Dot Apparatus (Biorad). The membrane was cross-linked twice at 120,000 microjoules/cm^2, washed 5 min with PBS-T solution, blocked in 5% milk and then hybridized with m6A-antibody overnight at room temperature. After three washes in PBS-T, the filter was hybridized with the rabbit secondary antibody for one hour at room temperature.

Detection was performed with Clarity Max Western ECL Blotting Substrate (BioRad) using ChemiDoc MP System and images were analyzed using Image Lab Software (BioRad).

Plasmids Construction

P-circ and the p-lin construction was already described by Legnini et al. (2017). The plasmids in that study are named as "p-circ3xF" and "p-lin-3xF," respectively.

We obtained the c-Δ1 mutant by inverse PCR followed by ligation, from p-circ and p-lin, respectively, with Δ1_fw and Δ1_rev oligos; the c-Δ2 and the l-Δ2 mutants with Δ2_fw and Δ2_rev oligos; the c-Δ3 mutant with Δ3_fw and Δ3_rev oligos.

In order to obtain c-Δαβ, c-Δαβ2 and l-Δαβ2 mutants, p-circ, p-lin, c-Δ2 or l-Δ2, respectively, were first linearized by inverse PCR with Δαβ_Inverse_fw and Δαβ_Inverse_rev oligos. The insert containing the desired mutations was obtained by annealing ssDNA oligos Δαβ_Insert_fw and Δαβ_Insert_rev; the insert was introduced in the linearized vectors with the In-Fusion® HD Cloning (Clontech) kit, according to manufacturer's instructions. The plasmids were amplified in DH5α competent cells (Thermo Fisher Scientific)

The construct overexpressing Flag-tagged YTHDF3 was kindly provided by Dr. Chuan He group. The construct overexpressing Flag-tagged EIF4G2 was bought from Sino Biological Inc. [HG16622-CF].

M(6)A CLIP

M^{6}A CLIP was performed according to the protocol described by Linder et al. (2015) with some modifications. Briefly, total RNA was purified from HeLa cells, 20 μg of RNA were diluted in IP buffer supplemented with RNase Inhibitor (Thermo Fisher Scientific) and incubated with 5 μg of anti-m6A antibody for 2hrs at 4°C rotating head over tail and crosslinked, 10% of the solution was saved to be used as input, the leftover incubated with protein A/protein G dynabeads (Thermo Fisher Scientific) for 2hrs at 4°C. Bead-bound antibody-RNA complexes were washed and recovered. After phenol-chloroform extraction and precipitation, RNA was resuspended in 30 μL and 7 μL were reverse-transcribed with VILO Superscript (Thermo Fisher Scientific) in a 10 μL reaction. q-PCR was performed to evaluate targets enrichment.

Immunoprecipitation

HeLa cells (600X10^3) were transfected in a 35mm plate with either a control plasmid or with the plasmid overexpressing the flag-tagged protein of interest and transferred to a 10cm plate 12hrs later. 48hrs later, cells were washed twice with PBS buffer and scraped with an IP buffer (20mM TrisHCl pH7.5, 150mM NaCl, 15mM MgCl2, 0.5% NP40, 1mM EDTA, DTT 1 μM, PIC (Roche) 1x. Lysates were incubated for 5min on ice and then passed through a 21G needle.

Lysates were spun down for 15min at 4°C at 13000 rpm and the supernatants were collected. 500ug-1mg of extract quantified through a Bradford assay were diluted in 1,5 mL of IP buffer and incubated with 10 μg of tRNA and 60μL Anti-FLAG Magnetic Beads (Sigma M8823) (washed twice with the Ip buffer) and incubated 3hrs-overnight at 4°C on a wheel. The 10% of the used extract was saved to be used as input. The beads were recovered through a magnetic rack and washed four times with 1ml wash buffer1 (20mM TrisHCl pH7.5, 200mM NaCl, 15mM, MgCl2, 0.5% NP40, 1mM EDTA). Samples collected after the last wash were divided for protein

or RNA analysis. The proteins fraction was resuspended in LDS 1X buffer (Biorad) added with DTT 1 μM, heated at 95°C for 10 min and loaded for western blot analyses. The RNA was extracted and reverse transcribed with VILO Superscript (Life Technologies) for qPCR analyses.

RNA-Seq

Total RNA was extracted from two biological replicates of HeLa cells treated with siRNA against either YTHDC1 or METTL3. Two biological replicates of the control sample were produced for the knock-down of YTHDC1 and one for the knock-down of METTL3. The RNA library was produced using Truseq Stranded Total RNA kit with Ribo-Zero H/M/R treatment (Illumina) and sequenced on an Illumina Novaseq6000 Sequencing system. An average of about 33.5 million 101 nucleotides long paired-end read pairs were produced for each sample.

Bioinformatic Analyses

YTHDC1 RIP-Seq (Roundtree et al., 2017) raw data (input and IP Ribo(-) from HeLa cells) and m^{6}A RIP (Zhou et al., 2017) (input, eluate, and supernatant from HeLa cells) were downloaded from GEO (GSE74397, GSE85324). Biological replicates from m^{6}A-RIP were pooled to improve circRNA detection sensitivity.

Trimmomatic (Bolger et al., 2014) and Cutadapt (Martin, 2011) were used to remove adaptor sequences in reads from knock-down and RIP-Seq experiments, respectively; minimum read length after trimming was set to 20. Reads were then aligned to the human reference genome (GRCh38) using BWA-MEM (Li, 2013) with *-T 19* option. circRNA detection in each sample was then carried out using CIRI2 software (Gao, Zhang and Zhao, 2018), which is able to identify circRNAs by searching for reads which map to back-splicing junctions. To identify circRNA host genes, the program was provided with Ensembl 90 gene annotation (Zerbino et al., 2018). For each back-splicing event found, CIRI2 reports the number of reads mapping to the back-splicing junction and on the corresponding linear splicing junctions, calculated summing all the reads mapping linearly on both the splice junctions involved in back-splicing; the latter are not reported if no read is assigned to the back-splicing junction, even if the circular RNA is detected in other samples. In order to count the reads mapping to linear splicing sites in samples in which no reads where mapped to corresponding back-splicing junctions detected in other samples, alignment files from each sample were modified by adding reads mapping to circRNAs found only in other samples and CIRI2 was rerun on these files. Putative back-splicing events that were spanning two non-overlapping genes, which were likely to be due to mapping errors, were excluded from further analysis.

Reads mapping to back-splicing junctions and to their cognate linear splicing junctions were converted to Count Per Million (CPM) values using edgeR R package (Robinson et al., 2010) and used for circRNA and linear RNA quantification. To evaluate the differential expression of circRNAs between knock-down and si-scramble conditions, we provided the edgeR software with the read counts of both the back-splicing events and their cognate linear splicing events. Events not having 2 or more counts in at least one sample were not tested for differential expression. Model fitting and testing was performed using the glmFIT and glmLRT functions. Given the low number of reads used for testing, we decided to use p value instead of false discovery rate to select for differentially expressed events, setting the significance threshold value to 0.1.

CircRNAs enriched in YTHDC1 RIP were defined as those with a fold change over the input of at least 2. CircRNAs exclusively precipitated by m^{6}a RIP were defined as those having at least 2 counts in the eluate and none in the supernatant; those having at least 2 counts in the supernatant and none in the eluate were classified as non-precipitated.

M^{6}A antibody-enriched RNA regions and precise consensus m^{6}A sites identified via m^{6}a-CLIP on total RNA from nucleoplasm and cytoplasm, and PolyA+ RNA from cytoplasm of HeLa cells (Ke et al., 2017) were downloaded from GEO (GSE86336). Bedtools suite (Quinlan and Hall, 2010) was used to search for overlaps between m^{6}A antibody-enriched RNA regions and exonic regions from protein-coding transcripts included within circRNAs genomic coordinates.

QUANTIFICATION AND STATISTICAL ANALYSIS

All statistical tests, statistical significance for comparisons of means and sample numbers are disclosed in respective Figure Legends. Statistical analysis of bioinformatics data are described in details in the "Method Details" section.